Evidence for a Bilayer Quantum Wigner Solid

H. C. Manoharan,* Y. W. Suen, M. B. Santos, and M. Shayegan
Department of Electrical Engineering, Princeton University, Princeton, New Jersey 08544
(Received 20 February 1996)

As the electronic charge distribution in a wide quantum well is tuned from a monolayer through an interacting bilayer configuration toward weakly coupled parallel layers, we observe an insulating phase concurrently manifesting a dramatic evolution. The data reveal that both interlayer interactions and charge symmetry, playing crucial roles, are able to stabilize a *correlated bilayer* electron insulator, thus providing tantalizing evidence of a pinned bilayer Wigner solid phase crystallizing at total filling factor ν as large as 0.54 ($\nu > \frac{1}{4}$ in each layer). [S0031-9007(96)01085-X]

PACS numbers: 71.45.–d, 73.20.Dx, 73.40.Hm

It is possible to fundamentally alter the many-body ground states of a two-dimensional electron system (2D ES) at high magnetic fields (B) through the introduction of an additional degree of freedom. For example, the addition of a spin degree of freedom enables the formation of particular spin-unpolarized fractional quantum Hall (FQH) states observed at lower B [1,2], while radically increasing the perpendicular spatial degree of freedom leads to a weakening and eventual collapse of the FQH effect [3,4]. Here we report magnetotransport measurements on an interacting *bilayer* ES confined in a wide quantum well. In this system, the additional layer degree of freedom stabilizes new FQH states such as the even-denominator incompressible liquids at Landau level filling factors $\nu = \frac{1}{2}$ [5–7] and $\nu = \frac{3}{2}$ [6], which have no counterpart in standard single-layer 2D ESs. Our data reveal an intriguing interplay between the FQH effect and an insulating phase (IP) that displays behavior profoundly different from any observed in a standard 2D ES. In this paper we focus on this IP, which, we demonstrate, evolves into a *correlated bilayer* electron insulator with intralayer and *interlayer* interactions holding equal significance, thus providing unique evidence for a pinned bilayer Wigner crystal (WC).

The sample, grown by molecular beam epitaxy, consists of a 750 Å GaAs quantum well flanked by $Al_{0.35}Ga_{0.65}As$ spacers and Si δ-doped layers. When cooled to low temperature (T) in a dilution refrigerator, this sample has typical dark density $n \simeq 1 \times 10^{11}$ cm^{-2} and mobility $\mu \simeq 1 \times 10^6$ cm^2/V s. Both n and the charge distribution symmetry are controlled via frontside and backside gates [5,6,8]. In the density range spanned by our experiments, $3.7 \times 10^{10} < n < 19.0 \times 10^{10}$ cm^{-2}, at most two subbands are occupied. As electrons are added to the wide quantum well, their electrostatic repulsion causes them to pile up near the sides of the well, and the resulting electron distribution appears increasingly bilayerlike as n grows [Fig. 1 (inset)] [8]. For symmetric charge distributions, i.e., "balanced" states, two relevant parameters that quantify this evolution are the symmetric-to-antisymmetric energy gap Δ_{SAS}, which is a measure of the coupling between the two layers, and the interlayer distance d [Fig. 1 (inset)]. Experimentally, Δ_{SAS} is deduced from Fourier transforms of the low-B Shubnikov–de Haas oscillations at various n [5,6,8]. A crucial property of the ES in a wide quantum well is that, for a given well width, both Δ_{SAS} and d depend on n: Increasing n makes d larger and Δ_{SAS} smaller. Thus, by increasing n, the system can essentially be tuned from a (thick) single-layer-like system exhibiting the usual FQH effect at odd-denominator fillings to a bilayer ES, where for the highest n the strongest FQH states are those with *even numerators*, as expected for a system of two 2D layers in parallel. For intermediate n, *even-denominator* FQH states at $\nu = \frac{1}{2}$ and $\frac{3}{2}$, which are stabilized by both interlayer and intralayer correlations, are observed. Concurrent with this evolution of the FQH states, we observe an IP which moves to *higher* ν as n is increased.

The spectacular behavior of this IP is summarized in Fig. 1, where the diagonal resistivity ρ_{xx} at base T

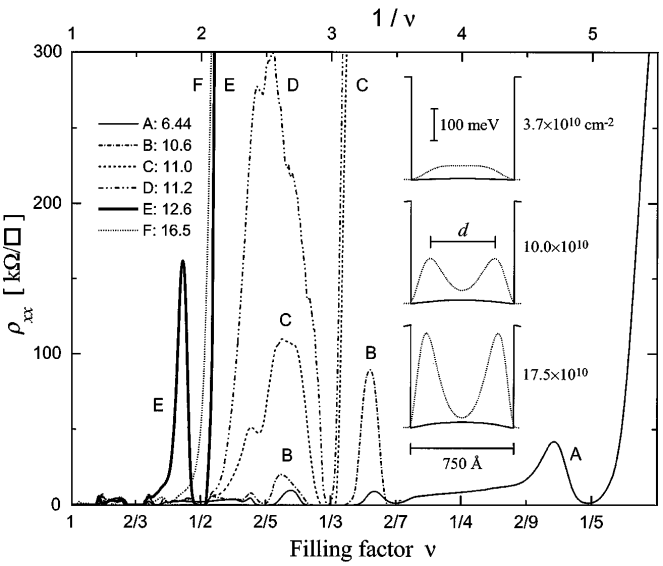

FIG. 1. Evolution of the IP at $T \simeq 25$ mK for varying n (specified in units of 10^{10} cm^{-2} within legend). Inset: Conduction band potentials (solid curves) and electron density profiles (dotted curves) from self-consistent Hartree-Fock simulations for increasing n.

($\simeq$25 mK) is plotted vs $\nu^{-1} \propto B$ for several representative n. Experimentally, the IP is identified by a ρ_{xx} that is both large ($> h/e^2 \simeq 26\ \mathrm{k}\Omega/\square$, the quantum unit of resistance) as well as strongly T dependent. For very low n, the IP appears near $\nu = \frac{1}{5}$ (trace A), while at the highest n there is an IP for $\nu \lesssim \frac{1}{2}$. The IP observed in the intermediate density range ($10 \times 10^{10} \lesssim n \lesssim 14 \times 10^{10}\ \mathrm{cm}^{-2}$) is most remarkable as it very quickly moves to larger ν with small increases in n (see, e.g., traces B, C, and D); along the way, it also shows *reentrant* behavior around well-developed FQH states at $\nu = \frac{2}{7}$ (trace B), $\nu = \frac{1}{3}$ (traces C and D), and $\nu = \frac{1}{2}$ (bold trace E). Then, as n increases past this point, the IP begins to move in the opposite direction to lower ν (trace F).

The data in Fig. 1 for $n = 12.6 \times 10^{10}\ \mathrm{cm}^{-2}$ are plotted in more detail in Fig. 2, along with the associated Hall resistivity and the T dependence of both the reentrant IP peak (showing a diverging ρ_{xx} as $T \to 0$) and the $\nu = \frac{1}{2}$ minimum (exhibiting activated behavior characteristic of a FQH liquid state with finite energy gap). As a whole, the data of Fig. 2 bear a striking resemblance to the IP observed reentrant around $\nu = \frac{1}{5}$ in low-disorder, single-layer 2D ESs, generally interpreted as a pinned Wigner solid [9]; here, however, the IP is reentrant around the bilayer $\nu = \frac{1}{2}$ FQH state, with the reentrant peak reaching the prominently high filling of $\nu = 0.54$.

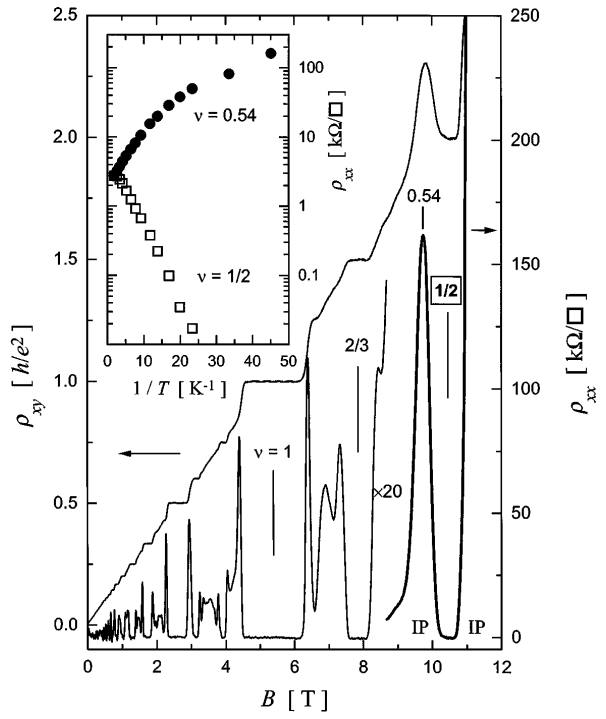

FIG. 2. Diagonal and Hall resistivity vs B at $n = 12.6 \times 10^{10}\ \mathrm{cm}^{-2}$, highlighting the reentrant IP around the bilayer $\nu = 1/2$ FQH liquid. Inset: T dependence of the $\nu = \frac{1}{2}$ minimum and the reentrant peak at $\nu = 0.54$.

The IPs presented in Fig. 1 cannot be explained by single-particle localization. First, in the case of standard, single-layer 2D ESs it is well known that as n is lowered, the quality of the 2D ES deteriorates and the sample shows a disorder-induced IP at progressively larger ν [10]. This is opposite to the behavior observed here: As n decreases from 19.0×10^{10} to $3.7 \times 10^{10}\ \mathrm{cm}^{-2}$, the quality worsens somewhat as expected (e.g., mobility decreases monotonically from 1.4×10^6 to $5.3 \times 10^5\ \mathrm{cm}^2/\mathrm{V\,s}$) but the IP moves to *smaller* ν. Second, the observation of IPs which are reentrant around *correlated* FQH states, and particularly around the very fragile and disorder-sensitive $\nu = \frac{1}{2}$ state [6], strongly suggests that electron interactions are also essential for stabilizing the IP.

To illustrate that the behavior of this IP is indeed consistent with the WC picture, it is important to elaborate on the evolution of FQH states in an ES confined in a wide quantum well [6]. This evolution can be understood by examining the competition between (1) Δ_{SAS} [11], (2) the in-plane correlation energy $Ce^2/\epsilon\ell_B$ [where C is a constant $\sim$0.1 and $\ell_B \equiv (\hbar/eB)^{1/2}$ is the magnetic length], and (3) the interlayer Coulomb interaction ($\sim e^2/\epsilon d$). To quantify the behavior it is useful to construct the ratios $\gamma \equiv (e^2/\epsilon\ell_B)/\Delta_{\mathrm{SAS}}$ and $(e^2/\epsilon\ell_B)/(e^2/\epsilon d) = d/\ell_B$. As n is increased, γ increases since both Δ_{SAS} and ℓ_B (for a FQH state at a given ν) decrease, and d/ℓ_B increases. Experiments show that when γ is small, the ES exhibits only "one-component" (1C) FQH states (standard single-layer odd-denominator states) constructed solely from the symmetric subband, while for large γ the in-plane Coulomb energy becomes sufficiently strong to allow the antisymmetric subband to mix into the correlated ground state to lower its energy, and a "two-component" (2C) state ensues. These 2C states, constructed out of the now nearly degenerate symmetric and antisymmetric basis states, come in two classes. For large d/ℓ_B, the ES behaves as two independent layers in parallel, each with density $n/2$; FQH states in this regime therefore have even numerator and odd denominator. For small enough d/ℓ_B, the interlayer interaction can become comparable to the in-plane interaction and a fundamentally new kind of FQH state becomes possible. Such a state has strong interlayer correlation and can be at even-denominator ν. A special example is the Ψ_{331} state associated with the $\nu = \frac{1}{2}$ FQH state observed in bilayer ESs with appropriate parameters [5–7].

We have determined the quasiparticle excitation gaps Δ_ν of several FQH states in the current system for several n via thermal activation measurements; these gaps are plotted vs γ in Fig. 3(a). As expected, we observe that increasing γ suppresses 1C states and enhances 2C states. Two states, $\nu = \frac{2}{3}$ and $\nu = \frac{4}{3}$, undergo a 1C to 2C phase transition with increasing γ [6], as evidenced by sharp minima in their gaps. The critical point for this transition, $\gamma \simeq 13.5$, matches the point where the gaps of other 1C

and 2C states emerge from zero. Surrounding this point is a region where the $\nu = \frac{1}{2}$ FQH liquid stabilizes. Note that, since this 2C state also possesses interlayer correlation (the 2C $\nu = \frac{2}{3}$ and $\frac{4}{3}$ states are simply $\frac{1}{3}$ and $\frac{2}{3}$ states in parallel layers), it exists only within a finite range of γ. The relevance of this plot to the IP is immediately highlighted by examining the three main reentrant peaks in Fig. 1 (from traces *B*, *D*, and *E*), which appear at $\nu = 0.30$, 0.39, and 0.54 for the IPs surrounding the $\nu = \frac{2}{7}$, $\frac{1}{3}$, and $\frac{1}{2}$ FQH states, respectively. The values of γ at these reentrant peaks are, respectively, 16.9, 16.3, and 16.5. The peak positions span a large range of ν, and yet the associated γ are remarkably similar. Moreover, at this value of $\gamma \simeq 16.5$, interlayer interactions are clearly important as this point is straddled by the 2C $\frac{1}{2}$ state in Fig. 3(a).

The construction of a phase diagram for the observed IPs facilitates a lucid connection between the IP evolution, the 1C to 2C transition, and the development of the $\nu = \frac{1}{2}$ liquid. To this end, we first collected a ρ_{xx} data set for a fairly dense grid of points in the n-B plane by incrementally changing n and sweeping B at base T. Next ρ_{xx} was mapped to a color interpolating between blue ($\rho_{xx} = 0$) and red ($\rho_{xx} \geq h/e^2$). Finally, using the

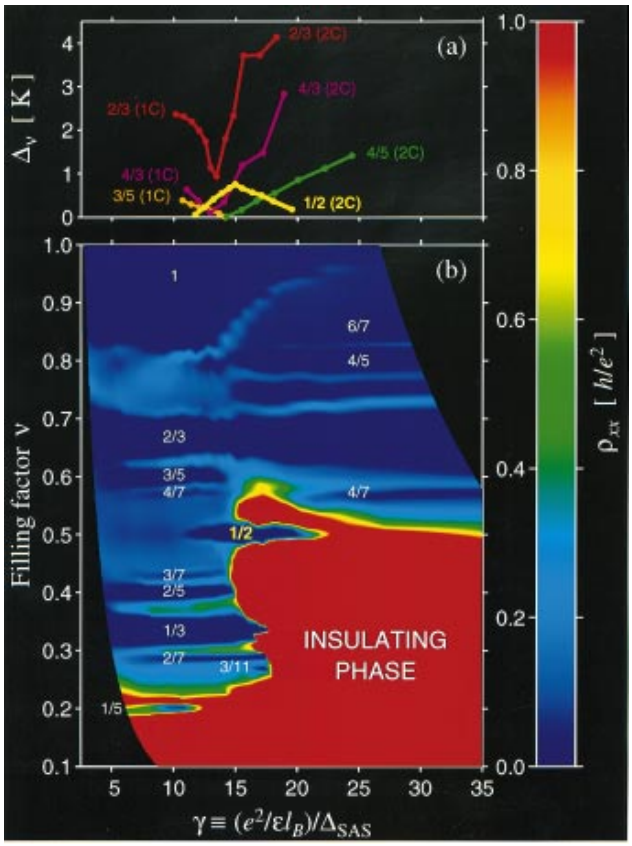

FIG. 3(color). (a) Measured energy gaps Δ_ν of several FQH states vs γ. The number of components (C) in each state is shown in parentheses. (b) Phase diagram showing ρ_{xx}, chromatically mapped according to the color bar (right), vs ν and γ.

B, n, and Δ_{SAS} values at each point, the color-mapped ρ_{xx} data set was plotted vs ν and γ [Fig. 3(b)]. By utilizing h/e^2 as a natural resistivity scale for demarcating the IP and noninsulating states [12], the result is a comprehensive phase diagram depicting incompressible phases (dark blue) together with compressible phases, both insulating (dark red) and metallic (all other colors).

Immediately obvious in the phase diagram are the various FQH transitions, manifested by the appearance or disappearance of dark blue FQH phases at several ν (see, e.g., $\frac{3}{5}$, $\frac{4}{5}$, and the $\frac{1}{2}$ "gulf"), or by a change in vertical width of the FQH phase (see, e.g., $\frac{2}{3}$); these transitions correlate directly with the measured energy gaps [Fig. 3(a)]. Another striking feature is the wrinkling in the IP boundary: This is caused by the aforementioned IP reentrance around several FQH states, perhaps most picturesque near $\nu \simeq 0.55$ due to the formation of an IP "peninsula" above the $\frac{1}{2}$ gulf. The limiting critical ν at low n (low γ) is close to $\frac{1}{5}$, consistent with a low-disorder monolayer 2D ES. For the highest n when the ES is effectively two weakly coupled layers in parallel, one would expect (and our measurements on wider quantum wells directly indicate) that the IP boundary moves to $\nu \simeq \frac{2}{5}$, consistent with two high-quality independent layers becoming insulating near $\frac{1}{5}$ filling in each layer. As our system is tuned through *coupled* layers, however, the IP boundary moves vividly above both of these limits to $\nu \lesssim 0.55$, and then only at higher n does it begin to fall back toward the $\frac{2}{5}$ weak-coupling limit (lying outside the density limits of our current sample).

We can examine in more detail the evolution of the IP as depicted in the phase diagram of Fig. 3(b) by making comparisons to Fig. 3(a). For intermediate n, as γ increases, the IP first remains close to $\nu = \frac{1}{5}$ but then begins to move to higher ν in the range $12 < \gamma < 15$. This range is precisely bisected by $\gamma \simeq 13.5$ [Fig. 3(a)], where the 1C to 2C transition occurs. Then the IP moves very quickly to $\nu \simeq \frac{1}{2}$ as evidenced by the nearly vertical phase boundary at $\gamma \simeq 16$. As discussed earlier, and as evident from Fig. 3, this γ is centrally located in the parameter range in which the $\frac{1}{2}$ state stabilizes. A quick glance at the phase diagram underscores this central point: The γ extent of the $\nu = \frac{1}{2}$ gulf coincides directly with the rapid ν shift in the phase boundary of the insulator.

The most convincing evidence for the formation of a pinned bilayer lattice comes from perturbing the symmetric ("balanced") charge distributions. Intuitively, the strength of a bilayer WC should be diminished under unbalanced conditions due to incommensurability effects. This is indeed observed quite prominently in our system, and can be highlighted by examining the high-ν reentrant IPs. Figure 4 shows the effect of asymmetry on the IP reentrant around $\nu = \frac{1}{3}$ at *fixed* $n = 11.0 \times 10^{10}$ cm^{-2} and for varying n_t, where n_t is the electron density transferred from the back layer to the front by proper gate biasing

from the balanced condition. We construct an "imbalance" phase diagram by plotting ρ_{xx}, color mapped to the same scale shown in Fig. 3, vs n_t and B [Fig. 4(b)], and include in Fig. 4(a) three representative ρ_{xx} traces [horizontal slices through the phase diagram of Fig. 4(b)]. It is very clear that, while the 1C $\nu = \frac{1}{3}$ state is strengthened as expected, the IP is weakened by increasing imbalance $|n_t|$: The IP is most stable in a perfectly balanced state ($n_t = 0$) with a phase boundary at $B \simeq 10$ T, while the IP peak at $\nu = 0.38$ ($B = 12$ T) drops dramatically even for small imbalance $n_t = 4.6 \times 10^9$ cm^{-2} [Fig. 4(a)]. As $|n_t|$ is increased past $\simeq 7 \times 10^9$ cm^{-2}, the reentrant IP is destroyed ($\rho_{xx} < h/e^2$) and the $\frac{1}{2}$ state disappears; the phase boundary (which has now jumped to $B \gtrsim 14$ T) continues to be pushed back as n_t increases further [Fig. 4(b)]. For the IP reentrant around $\nu = \frac{1}{2}$ at $n = 12.6 \times 10^{10}$ cm^{-2}, the corresponding destabilization of the insulator (not shown here) occurs at an imbalance of less than 3% ($|n_t|/n \simeq 0.027$). In all cases, note that both the $\nu = \frac{1}{2}$ state and the reentrant IP are strongest in the balanced condition; asymmetry simultaneously destroys both the bilayer quantum liquid *and* the insulator—for example, the vertical boundaries of the red reentrant IP "island" closely match those of the dark blue $\frac{1}{2}$ liquid phase [Fig. 4(b)].

Recently, several theoretical papers have examined Wigner crystallization in 2D systems with an additional spatial degree of freedom by considering multiple [13], wide [14], and double [15] quantum wells. While extracting details of the bilayer lattice (see, e.g., Ref. [15]) is beyond the scope of our work, our observation of a 2C insulator at the large fillings we identify sharply resonates with the fundamental principle underlying these theoretical investigations [13–15]: There is an additional potential energy gain due to the interlayer Coulomb interaction, so that for equivalent layer densities a 2C WC can form at higher ν (e.g., $\nu \gg \frac{1}{5}$ per layer) than a 1C WC. In addition, interlayer coupling may concomitantly weaken the FQH effect, making a crossing of the liquid and solid ground-state energies even more favorable [13,14].

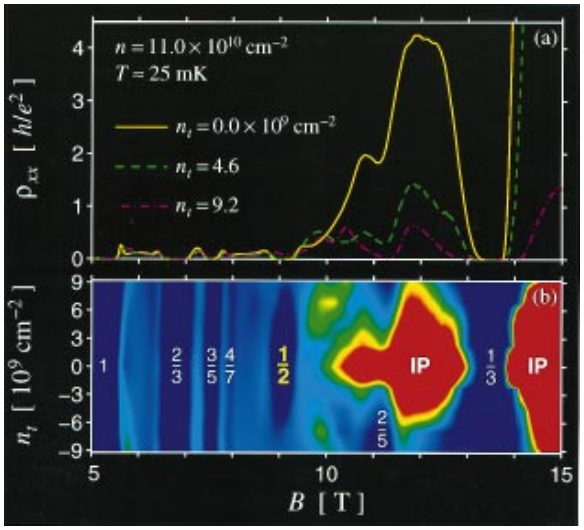

FIG. 4(color). Effect of asymmetry on the reentrant IP. Traces (a) and phase diagram (b) are at fixed total n, with varying amounts of charge n_t transferred between layers. [In (b), ρ_{xx} is mapped using the same color scale shown in Fig. 3.] Slight imbalance $|n_t|$ destabilizes the IP.

To summarize, our bilayer electron system provides a unique means of tuning the effective electron-electron interactions underpinning the formation of various many-particle ground states. The crux of this reasoning is that this system possesses two vital "yardsticks" for gauging the relative importance of interlayer and intralayer interactions: the 1C to 2C transition and the novel bilayer $\nu = \frac{1}{2}$ condensate. Utilizing these unimpeachable measuring sticks, we can connect the fascinating evolution of the IP with the significance and critical counterbalance of electron-electron interactions. In this light, our data conclusively indicate that the IP we observe for $\gamma \gtrsim 13$ is a collective 2C state with comparable interlayer and intralayer correlations. The characteristics of this bilayer electron insulator are remarkably consistent [13,14] with the formation of a novel pinned bilayer-correlated Wigner solid, a unique 2D electron crystal stabilized through the introduction of an additional quantum degree of freedom.

We thank X. Ying, S. R. Parihar, D. Shahar, and L. W. Engel for technical assistance. H. C. M. is grateful to the Fannie and John Hertz Foundation for fellowship support. This work was supported by the NSF.

*Electronic address: hari@princeton.edu

[1] R. Willett *et al.*, Phys. Rev. Lett. **59**, 1776 (1987).
[2] R. G. Clark *et al.*, Phys. Rev. Lett. **62**, 1536 (1989); J. P. Eisenstein *et al.*, *ibid.* **62**, 1540 (1989).
[3] M. Shayegan *et al.*, Phys. Rev. Lett. **65**, 2916 (1990).
[4] S. He *et al.*, Phys. Rev. B **42**, 11 376 (1990).
[5] Y. W. Suen *et al.*, Phys. Rev. Lett. **68**, 1379 (1992); **69**, 3551 (1992).
[6] Y. W. Suen *et al.*, Phys. Rev. Lett. **72**, 3405 (1994).
[7] The $\nu = \frac{1}{2}$ FQH state is also observed in bilayer ESs in *double* quantum wells [J. P. Eisenstein *et al.*, Phys. Rev. Lett. **68**, 1383 (1992)].
[8] Y. W. Suen *et al.*, Phys. Rev. B **44**, 5947 (1991).
[9] *Physics of the Electron Solid*, edited by S. T. Chui (International, Boston, 1994).
[10] T. Sajoto *et al.*, Phys. Rev. B **41**, 8449 (1990).
[11] Calculations indicate that Δ_{SAS} is reduced in a strong perpendicular B but by only a small percentage [M. Abolfath *et al.* (unpublished)].
[12] D. Shahar *et al.*, Phys. Rev. Lett. **74**, 4511 (1995).
[13] H. C. Oji *et al.*, Phys. Rev. Lett. **58**, 824 (1987); L. Świerkowski *et al.*, *ibid.* **67**, 240 (1991).
[14] R. Price *et al.*, Phys. Rev. B **51**, 2017 (1995).
[15] L. Zheng and H. A. Fertig, Phys. Rev. B **52**, 12 282 (1995); S. Narasimhan and T.-L. Ho, *ibid.* **52**, 12 291 (1995).